Journal of Power Sources 250 (2014) 174–180

Contents lists available at ScienceDirect

Journal of Power Sources

journal homepage: www.elsevier.com/locate/jpowsour

Enhanced photovoltaic performance of CdS quantum dots sensitized highly oriented two-end-opened TiO_2 nanotubes array membrane

Sheng Gao, Junyou Yang*, Ming Liu, Hongzhou Yan, Weixin Li, Jiaqi Zhang, Yubo Luo

State Key Laboratory of Materials Processing and Die & Mould Technology, Huazhong University of Science and Technology, 1037 Luoyu Road, Wuhan 430074, Hubei, China

HIGHLIGHTS

- Two-end-opened TiO_2 nanotubes array membrane (O-TNT) was fabricated by anodization.
- O-TNT can absorb more CdS nanoparticles than closed-ended TiO_2 nanotubes array membrane (C-TNT).
- Enhanced photovoltaic performance of CdS/O-TNT photoanode was observed.

GRAPHICAL ABSTRACT

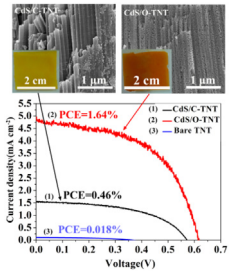

ARTICLE INFO

Article history:
Received 29 August 2013
Received in revised form
17 October 2013
Accepted 10 November 2013
Available online 19 November 2013

Keywords:
Titanium oxide
Two-end-opened structure
Cadmium sulfide
Power conversion efficiency

ABSTRACT

CdS quantum dots (QDs) sensitized highly oriented two-end-opened TiO_2 nanotubes array membrane solar cells have been fabricated in this paper. The structure, morphology and composition of the photoanodes have been characterized by XRD, SEM, TEM and EDX, respectively. It shows that the flow-through structure of two-end-opened TiO_2 nanotubes can absorb more CdS nanoparticles uniformly and prevent them from clogging at the nozzles of the nanotubes. The UV–Vis adsorption spectra also indicate that the CdS sensitized two-end-opened TiO_2 nanotubes have high absorbance than that of the closed-ended nanotubes. The photovoltaic parameters of the QDSSC based on the two-end-opened nanotubes array membrane are as follows: PCE = 1.64%, J_{sc} = 4.91 mA cm^{-2}, V_{oc} = 0.62 V and FF = 54.3%. The PCE value of 1.64% is about 3-fold enhanced in comparison with that of the QDSSC based on the closed-ended TiO_2 nanotubes array membrane.

1. Introduction

Nanostructured TiO_2 has been paid much attention in recent years due to its excellent properties, such as high stability, non-toxicity, good photocatalytic and photoelectric conversion performance [1,2]. Among various nanostructured TiO_2 materials, TiO_2 nanotubes (TNT), which have high surface-to-volume ratio and ordered one-dimensional (1D) structure, can offer a continuous pathway for photogenerated electrons to transport along the long axis of nanotubes and improve the charge collection efficiency [3]. TNT membranes have promising applications in many fields, such as photocatalytic degradation [4–6], photoelectrocatalytic hydrogen generation [7–13], dye sensitized solar cells (DSSCs) [14–20] and quantum dot sensitized solar cells (QDSSCs) [21–23]. Up to now, a variety of methods, such as anodic titanium oxide (ATO) [24,25], hydrothermal processes [26,27], sol–gel [28] and seeded growth [29], have been developed to prepare TNT membranes. Among them, the ATO method is considered as the most effective one due to its precise controllability to the pore diameter, wall thickness and nanotube morphology and length [4,6,13,30].

Generally, the bottom of TNT prepared by ATO method is closed and tightly bonded with the Ti substrate, and the closed bottom can

* Corresponding author. Tel.: +86 27 87558310.
E-mail addresses: jyyang@mail.hust.edu.cn, junyou.yang@163.com (J. Yang).

0378-7753/$ – see front matter © 2013 Elsevier B.V. All rights reserved.
http://dx.doi.org/10.1016/j.jpowsour.2013.11.015

be opened by chemical etching with acids. Liou et al. [31] immersed the TNT membrane into a 0.5% oxalic acid solution at 90 °C for 12 h and obtained an open-ended TNT membrane. Etching the closed bottom with HF vapors, Albu et al. [32] also reported a two-end-opened structure. Recently, it has been reported that two-end-opened TiO_2 nanotubes (O-TNT) can be prepared by increasing voltage for a short time at the end of ATO process [33,34]. The raising voltage can puncture the closed bottom and peel off the TNT array membrane from the Ti substrate automatically, and it is simple, environment friendly, and easy-controllable to obtain better TNT array membrane in comparison with the chemical etching method.

CdS is a narrow band gap semiconductor and has been widely studied as sensitizer for QDSSCs [35–37], photocatalysis [38,39] and etc [40,41]. In our previous work [42], CdS was deposited into a closed-ended TNT (C-TNT) membrane by a modified electrochemical atomic layer deposition for photocatalytic water splitting. Due to the closed-ended structure, it is difficult for QDs to reach the closed ends and attain a homogeneous coverage and sensitization to the TNT arrays because of the air resistance in the nanotubes, and the C-TNT membrane is easily clogged by the deposited quantum dots (QDs). However, to a two-end-opened structure, it is much easier to absorb the QDs without clogging the nanotube mouth due to its flow-through structure. Thus the two-end-opened structure is more preferable for the applications of QDSSCs and quantum dots sensitized photocatalysis. Recently, Liao et al. [33] reported a CdS sensitized two-end-opened TiO_2 membrane for photocatalytic application. However, up to now, less work has been reported on the application of two-open-ended TiO_2 membrane for QDSSCs.

In the present work, the C-TNT and O-TNT membranes have been fabricated by ATO method firstly, and then CdS QDS have been grown into them with the successive ionic layer adsorption and reaction (SILAR) method, respectively. The morphology, structure, optical absorption and photovoltaic properties of the CdS sensitized TNT photoanodes have been studied detailedly. A 3 times enhancement of the power conversion efficiency (1.64%) of the QDSSC based on a two-end-opened TNT membrane was achieved in comparison with that on a closed-ended TNT membrane.

2. Experimental section

2.1. Preparation of TNT membranes

TNT array membranes were prepared on a Ti foil using the potentiostatic anodization in a two-electrode electrochemical cell. All the anodization experiments were carried out at room temperature using a commercial available Ti foil (99.5% purity, 0.5 mm thickness) as the working electrode, a standard Pt electrode as the counter electrode. Before anodization, the Ti foil was chemical polished in a 1 vol.% HF aqueous solution for 2 min and cleaned by sonication in acetone, ethanol and distilled water consecutively for 30 min. Then the Ti foil was preanodized in an electrolyte composed of 0.3 wt.% NH_4F and 2 vol.% deionized water (DI water) in ethylene glycol at 60 V for 0.5 h. To avoid the nanowires occurring at the top of nanotubes, the preanodized Ti foil was annealed at 700 °C for 1 h. Subsequently, the annealed Ti foil substrate was anodized at 60 V for 10 h. For preparation of C-TNT array membranes, the reanodized Ti foil was annealed at 450 °C for 2 h and anodized again until the TNT array membranes peeled off from the Ti substrate. For preparation of O-TNT array membranes, the reanodized Ti foil was further anodized at 120 V for 4 min. The O-TNT array membranes were cleaned in ethanol and then annealed at 450 °C for 2 h.

2.2. Growth of CdS QDs and fabrication of QDSSCs

CdS QDs were grown into the TNT by the SILAR method. The TNT array membranes were firstly dipped into a 0.1 M $Cd(NO_3)_2$ aqueous solution for 5 min, rinsed with DI water for 1 min, then dipped into a 0.1 M Na_2S aqueous solution for 5 min and rinsed with DI water for 1 min. This dipping procedure was repeated for 4 cycles. After the deposition of CdS QDs, the TNT array membrane was then adhered onto an FTO glass with a binder of 0.1 M Ti-isopropoxide in ethanol. Then the adhered CdS/TNT/FTO was sintered at 350 °C for 0.5 h in air to get a good bonding. Subsequently, two more cycles were repeated to deposit CdS after which a ZnS passivation layer was further deposited in the CdS/TNT/FTO by alternatively dipping in a 0.1 M $ZnAc_2$ and a 0.1 M Na_2S aqueous solution for 4 cycles to avoid the corrosion of QDs and the recombination of injected electrons with holes in the electrolyte [43,44]. Then the QDSSCs were assembled with the ZnS/CdS/TNT/FTO photoanode, a Pt-coated FTO counter electrode and an iodide-based electrolyte, consisting of 0.1 M LiI, 0.12 M I_2, 1.0 M 1,2-dimethyl-3-propylimidazolium iodide (DMPII) and 0.5 M 4-*tert*-butylpyridine (4-TBP). The working area of the QDSSCs was 0.12 cm^2.

2.3. Characterization and measurements

The phase structure of the TNT and QDs were identified by X-ray diffraction (XRD, X'Pert PRO) with Cu Kα irradiation ($\lambda = 1.5406$ Å). The morphology and composition of the samples were characterized by a field-emission scanning electron microscope (FESEM, Nova NanoSEM 450) equipped with an energy dispersive X-ray spectrometer (EDX). The microstructure of the samples was observed by using a transmission electron microscope (TEM, JEOL JEM-2100). A spectrophotometer (Shimadzu UV-2550) was employed to record the UV–Vis spectra of samples. The current–voltage curves of the QDSSCs were measured under AM 1.5 G simulated sunlight illumination (100 mW cm^{-2}) using an electrochemical workstation (604D, CH Instruments).

3. Results and discussion

3.1. Morphology and structure of TNT array membranes

Fig. 1 shows the FESEM images of the free-standing TNT array membranes anodized at 60 V for 10 h. As seen from Fig. 1a, there are some cracks at the surface of the C-TNT membrane, and the inset in Fig. 1a shows an enlarged top morphology of the close-ended TNT, it can be seen that the average inner diameter of the nanotubes is about 100 nm. The cross-sectional image of the C-TNT (Fig. 1b) shows that the nanotubes are highly oriented with an average length of about 20 μm. The bottom view shown in Fig. 1c confirms that the nanotubes are close-ended in the bottom. After raising the voltage to 120 V for 4 min at the end of the anodization process, the closed-ended bottom was opened (Fig. 1d). Compared with the top view of the closed-ended TNT shown in Fig. 1a, the two-end-opened nanotubes are highly uniform and no crack can be seen at the surface. According to the forming principle of TNTs [1], the nanotubes are the product of two competitive processes of the field-assisted dissolution and the chemical dissolution. When the voltage is increased from 60 V to 120 V, a large number of F^- ions move directly to the bottom of TNT under high electric field and the dissolution at the bottom is greatly enhanced so that it can dissolve the barrier between TNT array membranes and Ti substrate [45]. With prolonging the time of dissolution, the barrier has been dissolved completely and then the O-TNT array membrane is formed and peeled off from the Ti substrate automatically. It is noteworthy

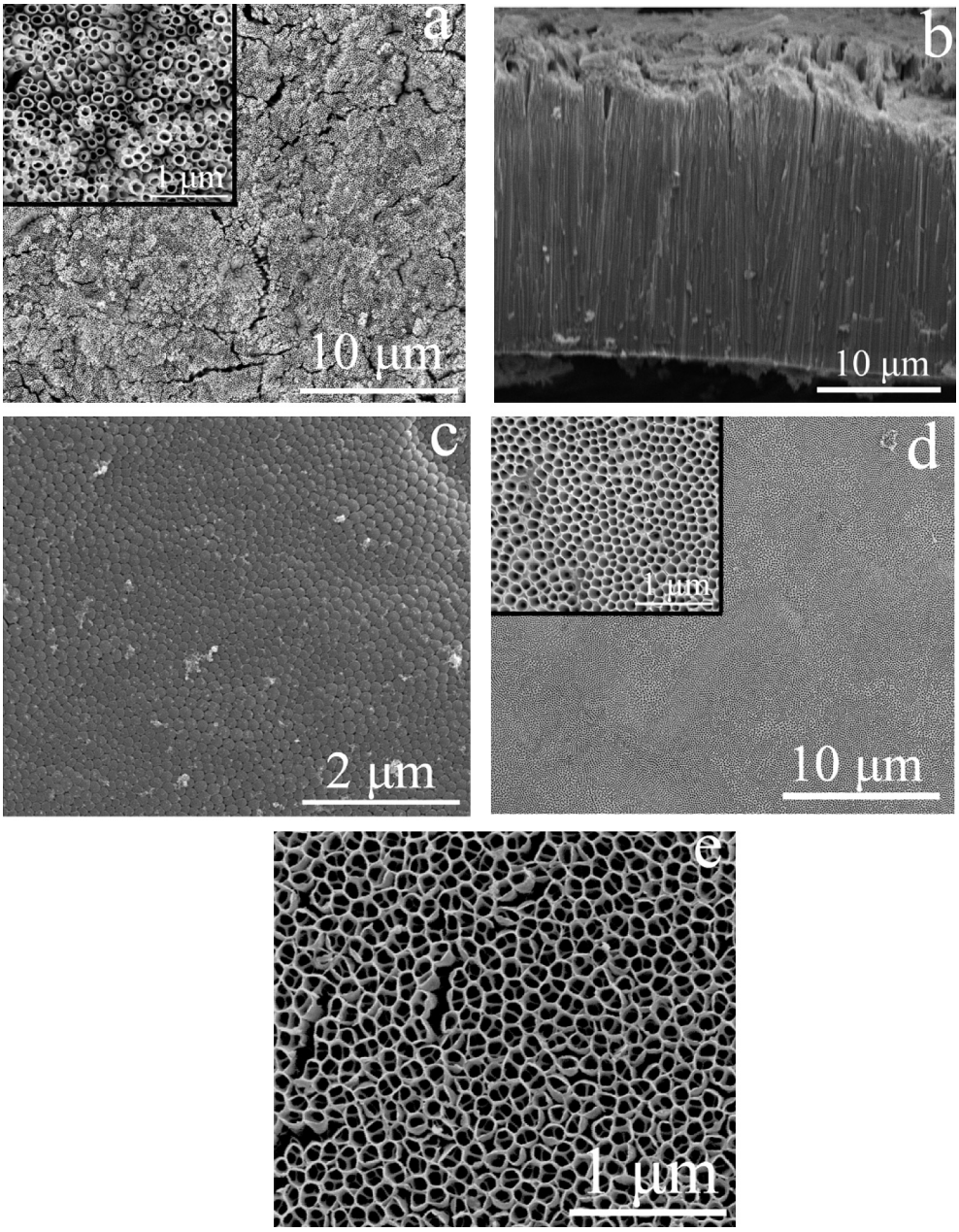

Fig. 1. FESEM top view (a), cross-sectional view (b), and bottom view (c) of the C-TNT membrane formed in ethylene glycol + 0.3 wt.% NH_4F + 2 vol.% H_2O at 60 V for 10 h anodization; and the bottom view (d) of the O-TNT after raising the voltage from 60 V to 120 V for 4 min. The insets in (a) and (d) are the magnification images of the C-TNT's top view and the O-TNT's bottom view, respectively; the FESEM top view (e) of the Ti substrate after the O-TNT's peeling off.

that another open-top TNT array membrane is left on the Ti substrate after the O-TNT's peeling off (Fig. 1e), so this process can be used for a continuous growth of O-TNT array membranes.

3.2. Morphology and structure of CdS sensitized TNT array membranes

XRD patterns of the bare TiO_2 nanotubes and CdS sensitized TiO_2 nanotubes are shown in Fig. 2. Obviously, the TNT array membrane has been fully converted to the photoactive anatase phase after calcination. Compared with the bare TiO_2, the CdS sensitized TiO_2 sample exhibits a new peak at 2θ about 28.10°, which can be indexed as the (1 0 1) peak of the hexagonal CdS (JCPDS No. 41-1049), indicating that CdS QDs are deposited successfully.

The morphologies of the CdS QDs sensitized TNT membranes are shown in Fig. 3, where Fig. 3a and b correspond to those of a close-ended TNT membrane, and Fig. 3c and d are of an open-ended membrane. As shown in Fig. 3a, CdS deposits aggregate at the top of nanotubes and most of the nanopores are clogged by them. It is conceivable that CdS nanoparticles cannot reach the lower part of the nanotubes and form a homogeneous coverage along the length of the closed-ended nanotubes. The cross-sectional image shown in Fig. 3b, in which very few CdS nanoparticles can be observed in the wall of the nanotubes, further confirms an inhomogeneous distribution of CdS QDs along the length of the closed-ended TNTs. However, as shown in Fig. 3c, the top view image of the QDs sensitized O-TNT array membrane is more uniform than that of the C-TNT membrane (Fig. 3a), and most of the nanopores on the top of

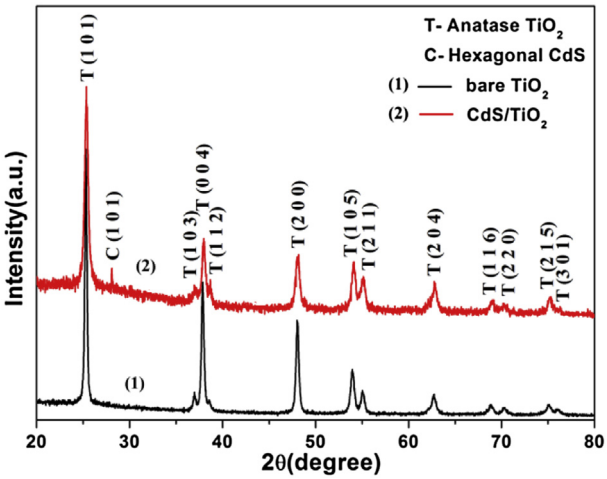

Fig. 2. XRD patterns of bare TiO_2 and CdS sensitized TiO_2.

the membrane are open and unblocked, indicating that more CdS nanoparticles distribute in the inner wall of the nanotubes. Noteworthily, as shown in Fig. 3d, CdS nanoparticles cover not only on the inner wall but also on the outer wall of TNTs evenly. This is because the chemical reaction between Cd^{2+} and S^{2-} can occur not only inside the TNTs, but also in the region between nanotubes. Thus a sandwich-like trilayer CdS/TNTs/CdS heterojunction is formed in this case. The EDX composition analysis of the CdS/O-TNT array membrane, shown in Fig. 3e, confirms that the atomic ratio of Cd to S is close to 1:1, which is in consistence with that of the stoichiometric CdS compound. The digital photos of the CdS/C-TNT and the CdS/O-TNT membrane are displayed in Fig. 3f and g, respectively. Apparently, the color of the CdS/O-TNT membrane is darker than that of the CdS/C-TNT membrane, indicating that the two-end-opened membrane can absorb more CdS QDs than the close-ended one in the same condition of SILAR.

The TEM micrograph of a CdS sensitized two-end-opened TiO_2 nanotube is shown in Fig. 4a. It can be seen that the nanotube is uniformly covered by CdS nanoparticles about 20 nm on both the

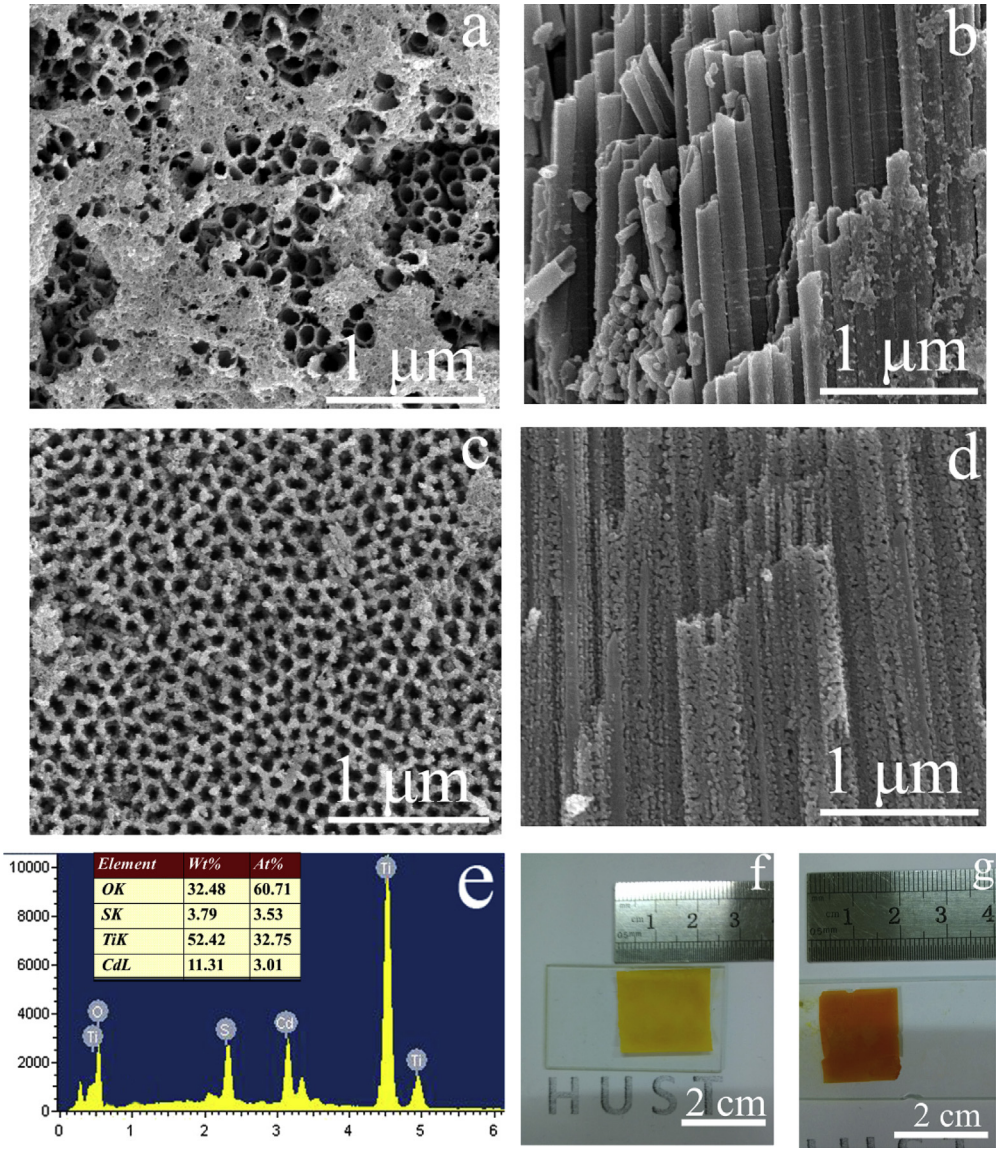

Fig. 3. FESEM images of (a) top view, (b) cross-sectional view of the CdS/C-TNT; (c) top view, (d) cross-sectional of the CdS/O-TNT; (e) EDX spectrum of the CdS/O-TNT; (f) and (g) the digital imagines of CdS/C-TNT and CdS/O-TNT, respectively.

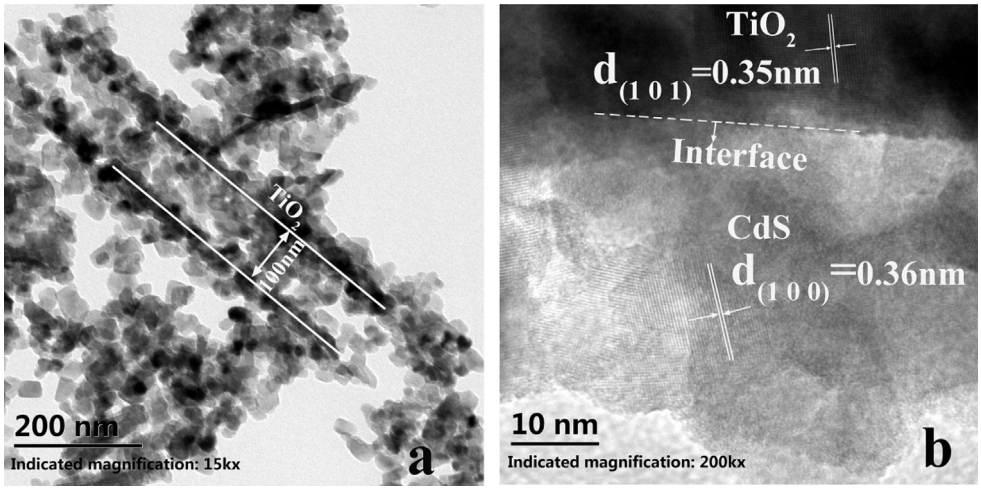

Fig. 4. (a) Low-magnified and (b) high-magnified HRTEM images of the CdS/O-TNT.

outer and inner walls along its length. The plane spacings of 0.35 nm and 0.36 nm, as labeled in the HRTEM imagine in Fig 4b, agree well with the (1 0 0) plane of CdS and (1 0 1) plane of anatase TiO_2, respectively.

Why is the coverage of CdS QDs on the two-end-opened nanotubes so different from that on the closed-ended nanotubes? To answer this question, a mechanism is proposed and schematically shown in Fig. 5. For the closed-ended TiO_2 nanotubes membrane, few Cd^{2+} cations and S^{2-} anions can enter deeply into the nanotubes during the alternative dipping process, because the residual air in the nanotubes prevents them from reaching the lower parts, while the Cd^{2+} cations and S^{2-} anions absorbed at the top surface react into CdS and accumulate during the alternative dipping process. Therefore, most of CdS nanoparticles aggregate at the top surface and clog the nozzles, and thus form an inhomogeneous coverage. In the case of the two-end-opened membrane, both Cd^{2+} and S^{2-} ions can be absorbed and react into CdS in the inner and outer wall of the nanotubes anywhere because the through-hole structure is free of air resistance, therefore CdS nanoparticles distribute uniformly on the walls of the nanotubes and the two-end-opened membrane can absorb more CdS QDs than the closed-ended one.

3.3. Optical absorption and photovoltaic properties

Fig. 6 shows the UV–Vis spectra of the bare TNT, CdS/C-TNT and CdS/O-TNT photoanodes, respectively. The bare TNT photoanode shows no absorption in the visible region due to its wide band gap (3.2 eV). After sensitization with CdS QDs, the absorption edge of both the CdS/C-TNT and the CdS/O-TNT extends to visible light region due to the narrow band gap (2.4 eV) of CdS. Furthermore, the absorbance of the CdS/O-TNT is higher in comparison with that of the CdS/C-TNT, indicating that more CdS nanoparticles have been deposited into the O-TNT which is in good consistent with the FESEM observation.

Fig. 7 shows the *J–V* curves of the QDSSCs with different TNT array membranes and their open circuit potential (V_{oc}), short circuit current density (J_{sc}), filling factor (FF) and power conversion efficiency (PCE) are listed in Table 1, correspondingly. The QDSSC based on bare TNT membrane produces a very low power conversion efficiency of about 0.018% because the bare TNT absorbs only 3–5% of the whole solar spectrum (UV-light), and the power conversion efficiency of QDSSC based on the CdS/C-TNT membrane is about 0.46%. Comparatively, the power conversion efficiency has increased to 1.64% when using the CdS/O-TNT membrane as the

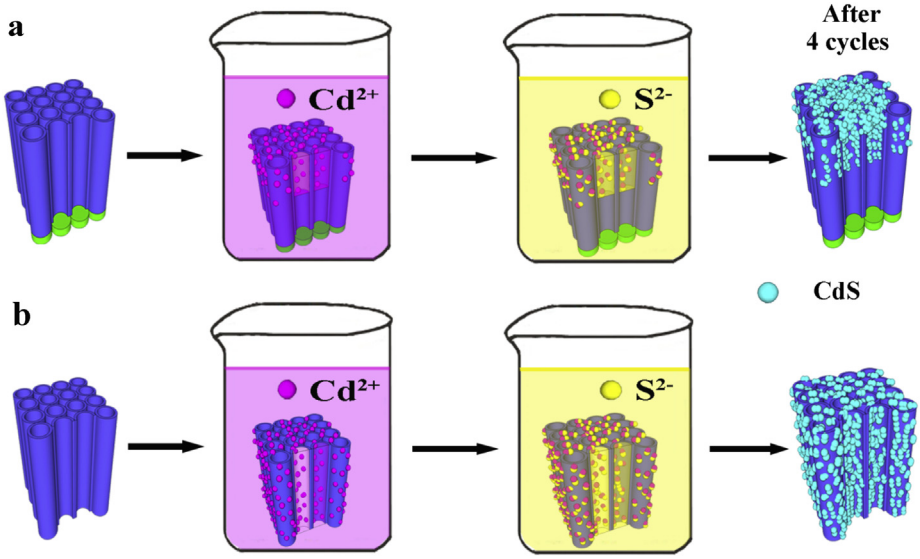

Fig. 5. Schematic illustration of the deposition of CdS QDs into (a) a closed-ended, and (b) a two-end-opened TNT membrane.

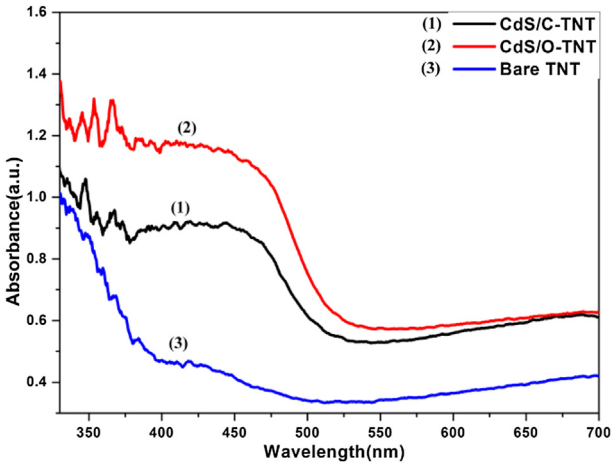

Fig. 6. UV–Vis absorption spectra of the CdS/TNT samples.

photoanode of QDSSCs, and achieves a 3-fold enhancement in comparison with that of the CdS/C-TNT membrane. The following reasons should be ascribed to the enhanced photoelectrical performance of the CdS/O-TNT QDSSC. Firstly, as confirmed by the above FESEM observation and UV–Vis spectrum, the O-TNT array membrane can absorb more CdS nanoparticles without blocking the mouths of nanotubes. The more CdS nanoparticles are absorbed, the more sunlight can be harvested, and therefore the higher power conversion efficiency is achieved. Secondly, the dense TiO_2 barrier at the bottom of the C-TNT membrane can filter some part of the sunlight leading to the decreasing of PCE. In addition, the dense TiO_2 barrier can also hinder the electrolyte from diffusing into the transition layer of TiO_2 nanoparticles thus resulting in the lower PCE in the QDSSC of CdS/C-TNT (The FESEM cross-sectional view of the transition TiO_2 nanoparticles layer is shown in Fig. S1).

Although the power conversion efficiency of the QDSSCs based on the CdS/O-TNT membrane is comparable with some reported CdS sensitized TiO_2 QDSSCs [43], it is still lower than QDSSCs based on some other sensitizers [23,46]. This should be attributed to the less effective visible light harvest of CdS QDs. Because the band gap of CdS is about 2.4 eV, and it limits the absorption range below the wavelength of about 550 nm. To further improve the photovoltaic performance, it is necessary to pay attention to the study of some narrower band gap sensitizers such as CdSe, PbS and co-sensitizers which have been proved to be more effective in visible light harvest. The related study is in progress and will be reported soon.

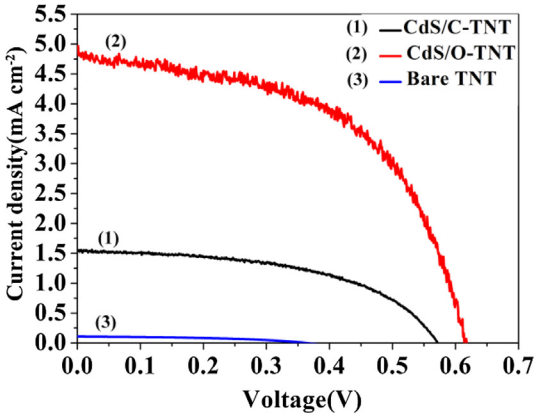

Fig. 7. *J–V* curves of the CdS/TNT samples with ZnS passivation layer.

Table 1
Photovoltaic performance parameters of the QDSSCs based on the CdS/C-TNT and the CdS/O-TNT photoanodes with ZnS passivation layer.

Photoanode	V_{oc} (V)	J_{sc} (mA cm^{-2})	FF (%)	PCE (%)
Bare TNT	0.36	0.11	44.7	0.018
CdS/C-TNT	0.57	1.55	52.2	0.46
CdS/O-TNT	0.62	4.91	54.3	1.64

4. Conclusions

In summary, we have fabricated a freestanding, highly oriented and two-end-opened TiO_2 nanotubes array membrane by anodization in this work. Thanking for the special two-end-opened structure, CdS QDs can be deposited uniformly on both the inner and outer walls of the nanotubes via the SILAR method. QDSSC based on the CdS/O-TNT has a power conversion efficiency of 1.64%, which is about 3-fold enhanced compared with that based on the CdS sensitized closed-ended TiO_2 membrane. This work confirmed the merit and potential of two-end-opened TiO_2 membranes for QDSSCs.

Acknowledgments

This work is co-financed by National Natural Science Foundation of China (Grant No. 51272080 and 51072062), National Basic Research Program of China (Grant No. 2013CB632500), Research Fund for the Doctoral Program of Higher Education, Ministry of Education of China (No. 20100142110016), Open Fund of State Key Laboratory of Advanced Technology for Materials Synthesis and Processing, Wuhan University of Technology (No. 2013-KF-3). The technical assistance from the Analytical and Testing Center of HUST is likewise gratefully acknowledged.

Appendix A. Supplementary data

Supplementary data related to this article can be found at http://dx.doi.org/10.1016/j.jpowsour.2013.11.015.

References

[1] G.K. Mor, O.K. Varghese, M. Paulose, K. Shankar, C.A. Grimes, Sol. Energy Mater. Sol. Cells 90 (2006) 2011–2075.
[2] A. Wold, Chem. Mater. 5 (1993) 280–283.
[3] J. Wang, Z. Lin, Chem. Asian J. 7 (2012) 2754–2762.
[4] D. Wang, Y. Liu, B. Yu, F. Zhou, W. Liu, Chem. Mater. 21 (2009) 1198–1206.
[5] H. Liu, G. Liu, X. Shi, Colloids Surf. A 363 (2010) 35–40.
[6] A. Mazzarolo, K. Lee, A. Vicenzo, P. Schmuki, Electrochem. Commun. 22 (2012) 162–165.
[7] C.W. Lai, S. Sreekantan, Electrochim. Acta 87 (2013) 294–302.
[8] W. Krengvirat, S. Sreekantan, A.M. Noor, G. Kawamura, H. Muto, A. Matsuda, Electrochim. Acta 89 (2013) 585–593.
[9] L. Sang, Z. Zhang, G. Bai, C. Du, C. Ma, Int. J. Hydrogen Energy 37 (2012) 854–859.
[10] E.Y. Kim, J.H. Park, G.Y. Han, J. Power Sources 184 (2008) 284–287.
[11] M. Ye, J. Gong, Y. Lai, C. Lin, Z. Lin, J. Am. Chem. Soc. 134 (2012) 15720–15723.
[12] L. Sang, H. Tan, X. Zhang, Y. Wu, C. Ma, C. Burda, J. Phys. Chem. C 116 (2012) 18633–18640.
[13] G.K. Mor, K. Shankar, M. Paulose, O.K. Varghese, C.A. Grimes, Nano Lett. 5 (2005) 191–195.
[14] M. Ye, D. Zheng, M. Lv, C. Chen, C. Lin, Z. Lin, Adv. Mater. 25 (2013) 3039–3044.
[15] L.-Y. Lin, C.-Y. Chen, M.-H. Yeh, K.-W. Tsai, C.-P. Lee, R. Vittal, C.-G. Wu, K.-C. Ho, J. Power Sources 243 (2013) 535–543.
[16] J.R. Jennings, A. Ghicov, L.M. Peter, P. Schmuki, A.B. Walker, J. Am. Chem. Soc. 130 (2008) 13364–13372.
[17] H. Park, C. Yang, W.-Y. Choi, J. Power Sources 216 (2012) 36–41.
[18] C.J. Lin, W.Y. Yu, S.H. Chien, J. Mater. Chem. 20 (2010) 1073–1077.
[19] J.-H. Park, J.-Y. Kim, J.-H. Kim, C.-J. Choi, H. Kim, Y.-E. Sung, K.-S. Ahn, J. Power Sources 196 (2011) 8904–8908.
[20] S. So, K. Lee, P. Schmuki, J. Am. Chem. Soc. 134 (2012) 11316–11318.

[21] X. Ma, Y. Shen, G. Wu, Q. Wu, B. Pei, M. Cao, F. Gu, J. Alloys Compd. 538 (2012) 61–65.
[22] Q. Shen, Akari Yamada, S. Tamura, T. Toyoda, Appl. Phys. Lett. 97 (2010) 123107.
[23] Y. Lai, Z. Lin, D. Zheng, L. Chi, R. Du, C. Lin, Electrochim. Acta 79 (2012) 175–181.
[24] D. Gong, C.A. Grimes, K. Varghese, W. Hu, R.S. Singh, Z. Chen, E.C. Dickey, J. Mater. Res. 16 (2001) 3331–3334.
[25] Y. Ji, K.C. Lin, H. Zheng, J. Zhu, A.C.S. Samia, Electrochem. Commun. 13 (2011) 1013–1015.
[26] T. Kasuga, M. Hiramatsu, A. Hoson, T. Sekiro, K. Niihara, Langmuir 14 (1998) 3160–3163.
[27] Q. Chen, W. Zhou, G. Du, L.M. Peng, Adv. Mater. 14 (2002) 1208–1211.
[28] S. Kobayashi, N. Hamasaki, M. Suzuki, M. Kimura, H. Shirai, K. Hanabusa, J. Am. Chem. Soc. 124 (2002) 6550–6551.
[29] Z.R. Tian, J.A. Voigt, J. Liu, B. Mckenzie, H. Xu, J. Am. Chem. Soc. 125 (2003) 12384–12385.
[30] C. Lin, S. Chen, L. Cao, Mater. Sci. Semicond. Process. 16 (2013) 154–159.
[31] Y.H. Liou, L.C. Kao, M.C. Tsai, C.J. Lin, Electrochem. Commun. 15 (2012) 66–69.
[32] S.P. Albu, A. Ghicov, J.M. Macak, R. Hahn, P. Schmuki, Nano Lett. 7 (2007) 1286–1289.
[33] J. Liao, S. Lin, N. Pan, D. Li, S. Li, J. Li, Chem. Eng. J. 211–212 (2012) 343–352.
[34] G. Liu, N. Hoivik, K. Wang, H. Jakobsen, J. Mater. Sci. 46 (2011) 7931–7935.
[35] T. Ganesh, R.S. Mane, G. Cai, J.H. Chang, S.H. Han, J. Phys. Chem. C 113 (2009) 7666–7669.
[36] Y.H. Lee, S.H. Im, J.H. Rhee, J.H. Lee, S. Seok, ACS Appl. Mater. Inter. 2 (2010) 1648–1652.
[37] N. Balis, V. Dracopoulos, E. Stathatos, N. Boukos, P.A. Lianos, J. Phys. Chem. C 115 (2011) 10911–10916.
[38] S. Feng, J. Yang, M. Liu, H. Zhu, J. Zhang, G. Li, J. Peng, Q. Liu, Electrochim. Acta 83 (2012) 321–326.
[39] H. Wang, Y. Bai, H. Zhang, Z. Zhang, J. Li, L. Guo, J. Phys. Chem. C 114 (2010) 16451–16455.
[40] T. Shanmugapriya, P. Ramamurthy, J. Phys. Chem. C 117 (2013) 12272–12278.
[41] S.H. Hwang, C.C. Moorefield, P. Wang, K.U. Jeong, S.D. Cheng, K.K. Kotta, G.R. Newkome, J. Am. Chem. Soc. 128 (2005) 7505–7509.
[42] W. Zhu, X. Liu, H. Liu, D. Tong, J. Yang, J. Peng, J. Am. Chem. Soc. 132 (2010) 12619–12626.
[43] S.-H. Hsu, S.-F. Hung, S.-H. Chien, J. Power Sources 233 (2013) 236–243.
[44] H.J. Lee, J. Bang, J. Park, S. Kim, S.-M. Park, Chem. Mater. 22 (2010) 5636–5643.
[45] G. Liu, K. Wang, N. Hoivik, H. Jakobsen, Sol. Energy Mater. Sol. Cells 98 (2012) 24–38.
[46] Y.-L. Lee, Y.-S. Lo, Adv. Funct. Mater. 19 (2009) 604–609.